Experimental and Molecular Dynamics Studies on the Consolidation of Hong Kong Marine Deposits under Heating and Vacuum Preloading

Chen, Ze-Jian (Ph.D. Candidate)
Department of Civil and Environmental Engineering, The Hong Kong Polytechnic University, Hong Kong SAR, China

Feng, Weiqiang (corresponding author) (Assistant Professor)
Department of Ocean Science and Engineering, Southern University of Science and Technology, Shenzhen, China.
Southern Marine Science and Engineering Guangdong Laboratory (Guangzhou), Guangzhou, China.
Email: fengwq@sustech.edu.cn

Li, An (Ph.D. Candidate)
Department of Civil and Environmental Engineering, The Hong Kong Polytechnic University, Hong Kong SAR, China.

Kamal Yahya Mohsen Al-Zaoari (Research Assistant)
Department of Ocean Science and Engineering, Southern University of Science and Technology, Shenzhen, China.

and
Yin, Jian-Hua (Chair Professor)
Department of Civil and Environmental Engineering, The Hong Kong Polytechnic University, Hong Kong SAR, China.
Research Institute for Land and Space, The Hong Kong Polytechnic University, Hong Kong SAR, China.

Manuscript Submitted to *Acta Geotechnica* for possible publication
as a technical paper

Abstract

Consolidation of marine soft soils with prefabricated vertical drains (PVDs) under vacuum preloading is a hot spot of research in marine geotechnical engineering. Marine soft soils are subject to low permeability and the consolidation is usually time-consuming. To accelerate the consolidation of marine soft soils, elevating the temperature with heating-aided PVDs in soils has been an attractive option. In this study, a series of laboratory tests were conducted to investigate the influence of heating on Hong Kong marine deposits (HKMD). Through the oedometer tests, the effects of heating on the compression and consolidation behaviour are quantified. In the two physical model tests with vacuum preloading, it is indicated that increasing the temperature to 40 °C in HKMD can significantly speed up the consolidation process, reduce vacuum loss, and increase the settlements and effective stress in a shorter period. The experimental study reveals that vacuum-heat preloading can be an effective method for the fast consolidation of marine soft soils. To reveal the mechanism of thermal effect on HKMD, the molecular dynamics simulation was performed with three typical mineral elements, and the thermal effect on the different responses of minerals in HKMD is interpreted. Furthermore, theoretical analysis with unit cell theory and simplified Hypothesis B method is also conducted for calculating the consolidation settlements of the model tests, with a quantified smear factor accounting for the combined effects of non-uniform consolidation, clogging, and temperature during vacuum-heat preloading.

Keywords: marine clay, consolidation, thermal effect, vacuum preloading, clogging, molecular dynamics

1 Introduction

In the past decades, marine infrastructure has played an important role in the economic development of human societies. In many coastal cities, the ground is covered with thick layers of marine soft soils that need to be treated before further construction. Such marine soft soils usually have high water content, low shear strength, high compressibility, and low permeability, which makes the consolidation process very complicated and time-consuming (Park et al. 2015; Yim 1994; Wu et al. 2020; Wang et al. 2021). The problem has become more challenging since many reclamation projects are being conducted to deal with the shortage of land supply in these regions, in which dredged marine soft soil has been proposed to be an important fill material due to the exhausted resources and sharply rising costs of natural sand.

Up to present, various techniques have been proposed and applied for accelerating the consolidation process of soft soils, including vacuum-preloading with vertical and horizontal drains (Chu et al. 2000; Chai et al. 2008; Zhang et al. 2014; Chai et al. 2014; Baral et al. 2021), dynamic drainage consolidation (Menard and Broise 1975; Deng and Xu 2010; Feng et al. 2017; Zhou et al. 2021), and electro-osmotic consolidation (Wan and Mitchell 1976; Bergado et al. 2003; Chien et al. 2009; Jeyakanthan and Gnanendran 2011). Among these techniques, vacuum preloading with prefabricated drains is considered a cost-effective way and has been frequently adopted in engineering. However, the effectiveness of vacuum preloading is adversely affected by the clogging effects, vacuum head loss, non-uniform consolidation, *etc.* (Indraratna et al. 2005; Wang et al. 2016; Perara et al. 2016; Zhou and Chai 2017; Xu et al. 2020).

To increase the efficiency of vacuum preloading, researchers have developed and applied different innovative methods, such as modification of soils (Wang et al. 2017; Wang et al. 2019; Sun 2020), electro-osmotic acceleration (Wang et al. 2018), and heating (Abuel-Naga et al. 2006;

Jarad 2016). Since the viscosity of pore water in the soil decreases with temperature, the permeability and consolidation coefficient of clayey soils will be increased under heating. Previous studies on Bangkok clay have demonstrated that under vacuum preloading with and without surcharge, heating the soils up to 90 °C can obviously increase the speed of consolidation (Saowapakpiboon et al. 2009; Artidteang et al. 2011). It was also indicated that such improvement is not obvious when the temperature exceeds 70 °C (Delage et al. 2000; Du et al. 2021). Regardless of the striking evidence showing the benefits of vacuum-heat preloading on dredged marine soils, several practical issues remain to be addressed. The concerns about energy consumption for high-temperature control have hindered its application (Wang et al. 2020; Du et al. 2021). It was indicated though, that heating below 60 °C can actually save energy due to the reduction of working time for the vacuum pump. The potential utilization of solar energy for heating the large-area construction field also restricts the temperature level. Therefore, it would be much more practical to focus on the effects of a temperature within a reasonable range, such as 30 to 40 °C. Furthermore, as an important factor in the efficiency of consolidation using vacuum preloading, the loss of vacuum pressure and clogging in the soil under different temperatures are still scarcely studied. Finally, study on the vacuum-heat preloading for Hong Kong Marine deposit or similar marine soils near the South China Sea is still a blank, although numerous schemes of reclamation or coastal development have been proposed for the near future around this area.

In this study, a systematic study was performed on the thermal consolidation of HKMD, including the experimental study and theoretical analysis, as shown in Fig. 1. Two thermal oedometer tests and two small-scale physical model tests were carried out to investigate the effects of heating on the basic properties of HKMD and vacuum preloading process of HKMD slurry. To reveal the mechanism of heating on HKMD, the molecular dynamics simulation was performed with three typical mineral elements. The thermal effects on the microstructures of marine soils are discussed. Finally, a theoretical analysis for the settlement of HKMD under vacuum-heating preloading in the two models is conducted using the parameters from the oedometer tests. The thermal effects on the smear factor F_s accounting for the clogging and non-uniform consolidation are revealed and discussed.

2 Experimental Design and Procedures

2.1 Test apparatus

(a) Thermal oedometer test

The thermal oedometer tests were performed in a modified oedometer cell which allows constant temperature control from 20 to 40 °C. Fig. 2 shows the schematic diagram of the modified oedometer. The system comprises a Wykeham Farrance conventional oedometer apparatus, a silicone tube, a temperature sensor, and a water bath with a peristaltic pump to circulate water inside the silicone tube. To avoid disturbing the specimens, the temperature sensor was placed in the water surrounding the specimen to measure the temperature of water to reflect the temperature in the soil specimen. This heating system could ensure that the water temperature is maintained within ± 0.1 °C of the set temperature throughout the test period.

Calibration tests were conducted to determine the correlation between temperatures in the soil specimen and the surrounding water in the oedometer cell. Two temperature sensors were inserted simultaneously into the center of the soil specimen and surrounding water respectively and maintained for 24 hours under a constant preset temperature. After the balance of temperature, the temperature sensor inside the soil specimen was changed to different positions. The results show that the temperature of the surrounding water was always approximately 2 °C higher than the temperature in the center soil specimen during the experimental testing, and the temperature inside the soil specimen can be considered consistent. The deformation with the change of temperature for each oedometer system was also well calibrated, which is ± 0.006 mm/°C.

(b) Physical model test

A steel cylinder with height of 500 mm and inner diameter of 294 mm was used for the vacuum-heat preloading tests. A prefabricated vertical drain (PVD) with length of 500 mm, width of 100 mm, and thickness of 5 mm was installed at the center of the cylinder and fixed at the bottom. The PVD is an integrated type, with filter layer adhered to the plastic core, which can prevent twisting of the filter during the tests (Cai et al. 2017). The top of vertical drain was connected to a cylindrical chamber for collecting the water, followed with an electric vacuum pump to provide vacuum air pressure. A polyethylene membrane bag was cut and fixed on the edge of cylinder to form an air-tight and free-deformed boundary on the surface of the soil. Heating in the soils was implemented by an electric heating wire with total length of 2 m fixed at the edge of PVD on both sides. The heating wire was connected to a thermostat device with mini temperature sensors that can be embedded inside the soils for temperature control.

The instrumentation of the model is shown in Fig. 3, with four pore water pressure transducers (PPT) buried in the HKMD slurry before vacuum preloading and two LVDTs installed on the surface of the membrane to measure the real-time settlement. A tape ruler was attached to the inner wall of the water chamber for measuring the total volume of water pumped out from the soils. At the middle of PVD, mini plastic tubes were attached to the outer surface of the filter layer and connected to a vacuum gauge for measuring the vacuum pressure inside the model.

2.2 Test materials

In Hong Kong, the local marine clay (Hong Kong Marine Deposit, HKMD) was rarely utilized in reclamation projects due to the concern of post-construction settlement. However, with the increasing demand for marine reclamation and shortage of sand supply, using marine deposits as fill materials has become a rational choice and such practices have been undertaken in other cities such as Tianjin, Wenzhou, *etc* (Du et al. 2010; Cai et al. 2017). To date, relevant studies on the vacuum consolidation behaviour of HKMD and similar marine soils are very rarely reported. The particle size distribution curve of HKMD used in this study is shown in Fig. 4. It can be seen that as a typical marine silty clay, HKMD contains around 20 % of clay (particle size < 2μm) and 62% of silt (particle sized from 2 to 50μm).

2.3 Test procedures

(a) Thermal oedometer test

To investigate the hydro-mechanical behaviour of HKMD under the two temperatures, oedometer tests with constant temperature control were carried out. The HKMD slurry was prepared and consolidated in a small steel cylinder under vertical stress of around 20 kPa. After that, two specimens were taken out from the cylinder with a confining ring for the oedometer tests. The specimen was heated by circulation of hot water in the silicone tube surrounding the confining ring, as described in Fig. 2. After saturation and temperature balance, vertical loadings of 5, 10, 20, 50, and 200 kPa were applied through the lever system. For the 50 and 200 kPa stages, the loading was sustained for 7 days to determine the creep coefficient.

(b) Physical model test

Two model tests were carried out on HKMD using the physical model described above without and with heating, namely Model 1 and Model 2. The HKMD was firstly mixed thoroughly with water to make a slurry with water content of 100%. The inner wall of the cylinder was smoothened by grease coating to reduce the friction between the wall and the soil. The PVD with heating wires was fixed at the center of the model. Then the HKMD slurry was put inside the steel cylinder slowly to reach a thickness of around 450 mm, with sensors buried in the soils at the designed height. Finally, the model filled with HKMD slurry was covered with a layer of geotextile and membrane. The edge of the membrane was glued to the edge of the cylindrical tank to make sure a fully air-tight condition.

The slurry was set for self-weight consolidation in the lab for 4 days before vacuum pressure was applied. After that, the vacuum load was increased gradually from 0 to 50 kPa within one hour and sustained during the following days. For Model 1, the temperature was constant at around 20 °C during the whole test. For Model 2, the soil was heated to keep the temperature of T0=40 °C after two days of self-weight consolidation and then kept constant in the following period.

3 Test Results Analysis and Discussions

3.1 Soil properties from thermal oedometer tests

Fig. 5 shows two $e-\log\sigma_z^{'}$ curves of HKMD from oedometer tests under 20 and 40 °C for 24 hours consolidation. The normal compression lines (NCLs) of the two specimens are almost parallel, with a small difference in the vertical positions. Such results share similarities with previous research (Campanella and Mitchell 1968; Cekerevac et al. 2002; Jarad 2016), although the difference is not too obvious. The most possible reason is that the clay content of HKMD is not as much as those in the literature. Tsutsumi and Tanaka (2012) showed the temperature effects on the compressibility and permeability of two different clays. The higher plasticity index, the higher temperature sensitivity of $e-\log\sigma_z^{'}$ curves, while the temperature sensitivity of permeability was similar for different clays.

Fig. 6 shows the $e-\log t$ curves of HKMD under different loading stages at 20 and 40 °C. It is shown that the settlement curves for both samples exhibit creep after the primary consolidation. It can be also observed that heating will shorten the primary consolidation period at the same loading stage.

The vertical permeability of HKMD under different loading stages can be computed using Terzaghi's 1-D consolidation theory, in which Casagrande's logarithm of time method was used to determine the time for end of primary consolidation (t_{EOP}) for each stage. The curves of void ratio against vertical permeability k_v are plotted in Fig. 7. The logarithm of vertical permeability follows an approximately linear relationship with void ratio, which has been recognized and discussed in detail by previous studies (Tavenas et al. 1983). The $e-\log k_v$ curve of HKMD under 40 °C is on the left side and almost parallel to the $e-\log k_v$ curve under 20 °C, which indicates that heating can increase the permeability of HKMD. Under the same void ratio, as temperature increases, the viscosity of porewater decreases, the shear resistance from the particles is reduced, and therefore the hydraulic conductivity is improved. Such results are similar to the literature (Cho et al. 1999, 2012; Abuel-Naga et al. 2006; Delage 2009; Tsutsumi and Tanaka 2012; Jarad 2016).

3.2 Temperature distribution in Model 2

For Model 1, heating was not applied on the PVD, and it is assumed that temperature in soil was held for a constant value of around 20 °C in the laboratory environment. For Model 2, the heat was spread from the heating wire in the center to the edge of the model. Fig. 8 shows the measured temperatures at four different positions in Model 2, in which the final distribution of temperature is non-uniform in the model due to heat loss from the boundaries. Along the vertical direction, temperature at the bottom of soils is lower than the middle, while in the horizontal direction, temperature near the edge of the model was lower compared to the middle one. The temperature of T3, which is believed to be the least heated point, only reaches around 30 °C when T0 was kept 40 °C during the test. However, the temperature at T1 is much lower than T2, due to the heat loss at the insulated top surface.

The temperature of soils also changes with time during the consolidation process. For T2 and T3, the temperature under self-weight consolidation is lower than that with vacuum pressure. As the thermal boundary is unchanged, it can be inferred that the thermal conductivity is increasing with time, which causes the temperature gradient to decrease. The increase of thermal conductivity can be attributed to the reduction of water content and void ratio for saturated soils (Abuel-Naga et al. 2008; Abuel-Naga et al. 2009; Chen et al. 2018; Liu et al. 2021). For T1, the temperature exhibits a different trend, which can be attributed to the non-insulated boundary. However, since the total energy input is not measured, it is difficult to quantify the real-time thermal conductivity of the soil.

After a certain period of vacuum consolidation, there is less change of temperature with time in the soil. The combination of two different mechanisms may explain that. First of all, the void ratio of soils continues to decrease and the thermal conductivity of soil matric increases. However, under vacuum pressure, the water has a tendency of inward flow from the edge to the PVD, in another word, from the cooler zone to the warmer zone. The water flow causes heat convection in the reverse direction of the heat transmission from the PVD to the edge of the model. These two mechanisms are compensated during the vacuum consolidation.

3.3 Consolidation settlements

The deformation of soil is evaluated by two different approaches. The first one is to measure the volume of water pumped from the soil, which can reflect the total volume changes of the soils, as calculated by:

$$S = H_w \frac{\pi D_c^2 / 4}{\pi D_s^2 / 4 - bt} \tag{1}$$

where S is the total settlement of soil with assumption of 1-D strain condition, H_w is the height of water in water collection chamber, D_c is the diameter of the water chamber, D_s is the diameter of the soil in the physical model, b is the width of the PVD and t is the thickness of the PVD.

Fig. 9 shows the vertical displacement of HKMD in Model 1 and Model 2 calculated from water volume during the vacuum loading. It can be seen that the settlement of soil in Model 2 is significantly larger than that in Model 1 during the consolidation process. For the earlier stage, the consolidation rate of HKMD is less sensitive to temperature, probably because the permeability under high void ratio is very high in both models. However, with the ongoing consolidation, the void ratio and permeability were gradually reduced, and permeability became more sensitive to fluid viscosity and temperature effects. According to Fig. 9, the periods needed to achieve the same settlement, 111 mm for example, were 240 hours and 75 hours for 20 °C and 40 °C respectively. Heating has accelerated this process by 2/3 of time, which can make significant benefits to engineering applications.

Fig. 10 shows the vertical settlement curves of Model 1 and Model 2 measured by LVDTs on the surface of soils, which shows similar trends to Fig. 9. The settlement curves by different methods are fairly close, although the final vertical settlement measured by LVDTs is slightly larger, due to the uneven surface of the soil and pumped water remaining in the pipelines.

3.4 Pore water pressure

Under vacuum pressure, the pore water pressure u_w in the soil will become smaller than the hydrostatic pressure $u = \gamma_w z$ inside the model. Therefore, negative excess pore water pressure ($u_e = u_w - \gamma_w z$) will be generated, inducing the vertical effective stress increases.

Fig. 11 shows the development of pore water pressure with time during vacuum loading. Despite of several points of abnormal rising due to some accidental air leakage, the pore water pressure generally follows a decreasing trend with immediate resealing. Through comparison, it is clear that the reduction of pore pressure in Model 2 is much faster than in Model 1, similar to the trend of settlement. At the final stage, the pore water pressure in Model 2 is lower than that in Model 1, indicating the final effective stress is increased with temperature.

The measured pore water pressure also follows a depth-dependent distribution. The final pore water pressure of PPT-1 located at the top of soil is the highest, while the pore water pressure of PPT-3 and PPT-4 is lower for both models, except PPT-4 in Model 1 which exhibits an unusual lower pore water pressure than PPT-3. The measured data from PPT 2 at the middle height of soil are in the middle value.

3.5 Vacuum pressure loss at the PVD surface

Fig. 12 shows the measured vacuum pressure at the middle height of PVD (the position shown in Fig. 3) in the soil for both models. It should be noted that the measuring point is not inside the plastic core of the PVDs, but on the outer surface of the filter layer to reflect the effective loading applied on the surrounding soil. For both models, the measured vacuum pressure is smaller than the 50 kPa as controlled by the vacuum pump and decreases with time, indicating a significant loss of vacuum head. The loss of vacuum head in Model 1 is more serious than that in Model 2, which implies that heating can ease the vacuum loss and thus increase the final settlement and effective stress as revealed in previous sections. At the final stage, the absolute value of vacuum pressure of Model 1 is approximately 10 kPa smaller than Model 2, which coincides with the measured pore pressure of PPT2 in Fig. 11.

The phenomenon of vacuum loss has been noticed by previous researchers (Wang et al. 2018; Indraratna et al. 2005). The loss of vacuum pressure might be attributed to leakage of membrane sealing or intersection of natural macropores with drains (Indraratna et al. 2004). Besides, bending of PVD due to compression of soils will reduce the discharge capacity of the drainage channels and impede the transferring of vacuum pressure (Cai et al. 2017; Lin 2015). Last but not least, clogging effect will also cause reduction of suction head and vacuum efficiency under the ground (Indraratna et al. 2005). Clogging is caused by soil particles moving towards the drain under the suction effect. The clogging surrounding the drain will result in the formation of soil column with much lower permeability, which will cause reduction of water discharge capacity. In this study, since the vacuum pressure was measured by the mini plastic tube fixed on the surface of filter layer and covered with filter paper, instead of penetrated into the core (Cai et al. 2017), the loss of vacuum pressure will be dependent on the resistance from not only the plastic core, but also the filter layer.

3.6 Bending and clogging of PVD

Fig. 13 shows the condition of PVD after the vacuum preloading tests. The PVDs in both models were severely distorted. The length of PVD after Model 2 is smaller than that after Model 1 since its total settlement is larger. Both PVDs have 3 bending points along the whole length. The horizontal deformation of Model 2 is slightly larger, which makes the curvature of the bending points a bit higher than Model 1. As suggested by previous studies (Bergado et al. 1996; Lin 2015; Cai et al. 2017), the number and shape of bending will affect the water discharge and pressure loss in PVDs. The sharper bending angles, the higher vacuum loss. Therefore, the PVD bending-induced vacuum loss in Model 1 should be similar to, or even a bit less than Model 2, which is contradictory to the overall vacuum loss observed during the tests. Therefore, it can be inferred that the vacuum loss in this study should be is dominated by the clogging instead of the bending of PVD.

To investigate the effects of clogging in the filter layer, microscopic photos of the PVDs after tests were taken by an optical microscope, with typical samples shown in Fig. 14. According to the microscopic photos, the filter layer of PVD consists of multi-layered meshes constituted by fibers. After the vacuum preloading tests, the meshes are jammed with soil particles and clusters, which verified the clogging effect in both models. According to these photos, it is still difficult to tell the difference in the clogging phenomenon between Model 1 and Model 2.

Fig. 15 shows an explanation for the clogging effect on vacuum loss. The horizontal cross-section of PVD consists of a plastic skeleton wrapped with a filter layer, and the water flow channel is formed between the plastic thin walls and the filter layer. Under vacuum preloading, the soils have a tendency of inward movement, which results in the formation of a soil column surrounding the PVD as well as clogging in the filter layer. Local vacuum loss will occur due to friction between water and the severely jammed filter layer, which is detected by the vacuum measurement tube attached on the outer surface of PVD. When the temperature is elevated in Model 2, the viscosity of water is lowered, which reduces the friction of the clogged layer and loss of suction head. Therefore, the measured vacuum pressure in Model 2 is larger than in Model 1.

3.7 Final water content and non-uniform consolidation

After the vacuum preloading, the membrane was removed, and the water content of HKMD was measured. The results can be found in Fig. 16. In general, the final water content in Model 1 is higher than in Model 2, which accords with the results of settlement in previous discussions.

As shown in Fig. 16, the final water content at the PVD in Model 1 is very low, compared to other positions. In vacuum preloading, non-uniform consolidation (soil column) surrounding the PVD is a common issue. The soil column exhibits extremely high density and low permeability, which impedes the water discharge from soils outside this region during the later period of consolidation. In Model 2, the uniformity of water content appears much better, which strongly indicates that heating can reduce the effect of non-uniform consolidation. The first reason might be that the permeability in the whole model is improved by heating, which helps the drainage of water from the soil to the drained boundary (*e.g.*, the PVD and the surface of soil). Besides, due to the heat concentration at the PVD, the permeability in the soil column is especially high, which further reduces the resistance against water flow. These factors all contribute to the increased uniformity of consolidation under higher temperatures. Although the water content in the soil column in Model 2 is not as low as in Model 1, the total water content in Model 2 is still significantly lower with a much shorter consolidation time due to the improved uniformity.

4 Molecular Dynamic Simulation of Thermal Effects on Clay Layers

4.1 Molecular dynamic simulation model

According to the experimental results, the consolidation of HKMD is significantly influenced by temperature in both oedometer and model tests. It is well known that increasing the temperature in soils will reduce the viscosity of free porewater and thus increase the permeability of soils, with well-established mathematical correlations between water viscosity and permeability

(Cho et al. 1999; Abuel-Naga et al. 2006; Wang et al. 2020). However, the specific reactions of clay particles and their influences on consolidation under changes of temperature are still unclear.

Molecular dynanmic simulations are complementary techniques for studying the complex structure and interlayer species interactions in clay particles (Cygan et al., 2009; Amarasinghe and Anandarajah, 2012; Chang et al., 1995). In this study, the crystallinity of HKMD was determined using the X-ray diffractometer (XRD, Rigaku Smartlab), and the microstructure was examined by Scanning Electron Microscope (SEM, Tescan VEGA3). The main minerals are Montmorillonite (MMT) and Kaolinate (Kao). The percentage of Montmorillonite in the total clay minerals of HKMD is 43%, and that of Kaolinate is 48%. Fig. 17 shows the microstructure of HKMD after the oedometer test. Three typical structures, MMT, Kao and MMT-Kao mixed layers are considered in the molecular dynamics simulation, as shown in Fig. 17.

The simulation was performed using Lammps software (Plimpton, 1995) and visualized using Ovito (Stukowski, 2009). The general chemical formula for the montmorillonite and kaolinite model can be described as Na0.75[Mg0.5Al3.5] (Si7.5Al10.25) $O_{20}(OH)_4$ and $Al_2Si_2O_5(OH)_4$, respectively (Ma et al., 2018). The structure of MMT is tetrahedral-octahedral-tetrahedral (T-O-T), whereas Kao has tetrahedral-octahedral (T-O) structure. The isomorphous substitution of Mg^{2+} atoms in the octahedral sheet replace Al^{3+} atoms in montmorillonite model. The montmorillonite model consists of three clay layers and two interlayers, whereas the kaolinite model consists of four clay layers. The mixed kaolinite- montmorillonite model consists of two MMT and Kao layers. In this study, a representative simulation cell with a reasonable size was selected through a convergence test. The size of the simulation cell for three models is 20.72 × 17.96 Å in the X and Y directions, and 69, 90.6, and 128.4 for Kao, MMT, and MMT-Kao respectively in the Z direction. The periodic boundary condition was applied in the three directions, in order to reduce the limitation brought by the scale effect and obtain reasonable simulations for the whole system with one representative cell (Amarasinghe and Anandarajah, 2013; Al-Zaoari et al., 2022).

The Simple Point Charge (SPC) water model (Berendsen et al., 1981) and CLAYFF force field (Cygan et al., 2004) were used to investigate interatomic interactions in this study. The CLAYFF force field has been demonstrated to be particularly successful in simulating clay mineral systems (Anderson et al., 2010), as well as their interfaces with water solutions. The clay models were first optimized to achieve a low-energy structure. Then, MD simulations in the NVE, NPT, and NPT ensembles for 20, 50, and 500 ps, respectively, were used to stabilize the system in the equilibrium process. Thereafter, the transition of absorbing water molecules along the clay surface and free water was recorded for 500 ps under the NPT ensemble.

4.2 Results and Discussion

Fig. 18 shows the trajectory lines of three water molecules with different initial locations. Their movements are tracked throughout the simulation. As shown in Fig. 19, the water density close to the clay mineral surface is higher than 1g/cm^3, which indicates that the water is at the adsorption state, whereas the density of free water is approximately 1g/cm^3. The thickness of the adsorption water on Kao's surfaces is about 9 Å for the tetrahedral surface and about 8 Å for the octahedral surface. According to the water molecular trajectory, some adsorbed water molecules transit to be free water, while some free water molecules adsorb on the clay surface to be the adsorption water. Furthermore, some adsorbed or free water does not transfer and remains in the same initial zone. Fig. 18 demonstrates that the adsorption water molecules on the clay mineral surface are not completely immobilized and that they transfer and exchange with pore water.

To investigate the thermal effect on the transition between adsorption state and free state, water density curves of MMT-Kao model at three different temperatures are simulated and compared in Fig. 19. The water density higher than 1g/cm^3 indicates the adsorption state. Fig. 19 shows that there are three layers of water adsorbing on the tetrahedral surface of MMT and Kao and two layers for Kao's octahedral surface, with a distance of about 9 Å, which can verify the thickness of the adsorption water on the clay surface. This result agrees with previous study (Ma et al., 2018). Furthermore, as the temperature rises, the adsorption water layers decrease from three water layers to two layers at 80°C, illustrating that higher temperature would help more adorption water transits into free water more quickly with a larger percentage.

The transit percentages of adsorbing water for MMT, Kao and MMT-Kao models are plotted in Fig. 20. It shows that roughly 70%, 60%, and 65% of initially adsorbed water transit to free water at the end of the simulation in MMT, Kao, and MMT-Kao, respectively. Furthermore, the transition percentage in MMT is higher than Kao, and the transition of water speeds up with increasing temperature in MMT and mixed structure (MMT-Kao) whereas this effect is not obvious for Kao. This may be attributed to the difference of the mineral structure: Kaolinite's octahedral surface has a greater attraction for water molecules, which can be seen by the higher peak density of water adsorbing in Fig. 19. Therefore, the adsorbed water molecules are not easy to transit even when the temperature increases.

The simulation results reveal that with higher temperatures, the thickness of adsorbed water layer is smaller. Therefore, the void ratio of HKMD at 40 °C will be smaller than HKMD at 20 °C under the same vertical effective stress, which explains the difference of normal compression lines for the two specimens in Fig. 5. Meanwhile, since the temperature effect on Kao is smaller than MMT, the temperature-dependency of NCL for HKMD is rather slight, compared to those reported in the literature (Abuel-Naga et al. 2007; Laloui et al. 2008), due to its relatively low percentage of clay minerals, especially MMT.

5. Theoretical analysis

5.1 Consolidation analysis under vacuum loading

The horizontal consolidation problem with PVD can be back-analyzed with the unit cell theory (Hansbo 1981), the simplified equation of which is shown in Eq.(2):

$$\bar{U}_h = 1 - \exp\left(-8T_h / \mu_s\right) \tag{2}$$

where $\bar{U}_h$ is the average degree of consolidation, $T_h = \frac{C_h t}{D^2}$ is the time factor for horizontal consolidation, $C_h = \frac{k_h}{m_v \gamma_w}$ is the coefficient of horizontal consolidation, $\mu_s = \ln\frac{n}{s} + \frac{k_h}{k_h^{'}}\ln s - \frac{3}{4}$, $m_v = \frac{\Delta\varepsilon_z}{\Delta\sigma_z^{'}}$ is the compressibility of soil, k_h is the horizontal permeability of soil in the non-smear zone, $k_h^{'}$ is the horizontal permeability of soil in the smear zone, $n = \frac{D}{d_w}$, $s = \frac{d_s}{d_w}$, D is the diameter of soil, d_s is the diameter of smear zone, d_w is the equivalent diameter of well (PVD), which is calculated as $d_w = 0.5b + 0.7t = 53.5$ mm (Long and Covo 1994).

The value of m_v can be calculated by the $e - \log\sigma_z^{'}$ curve. Since the HKMD in the physical models was not pre-consolidated before the tests, the soils can be regarded as normally consolidated soils. As shown in Fig. 5, the full NCL can be expressed by $e = N - C_c \log\sigma_z^{'}$, where N is the void ratio when $\sigma_z^{'} = 1$ kPa . Therefore, m_v can be calculated by $m_v = \frac{\Delta\varepsilon_z}{\Delta\sigma_z^{'}}$

$= \frac{\frac{C_c}{1+e_0}\log\frac{\sigma_z^{'}}{\sigma_{z0}^{'}}}{\sigma_z^{'}-\sigma_{z0}^{'}}$, where $e_0 = 2.65$ is the initial void ratio, C_c is the normal compression index, $\sigma_{z0}^{'}$ and $\sigma_z^{'}$ is the initial and final vertical effective stress of soil.

Similarly, the value of k_v can be obtained from the $e-\log k_v$ in Fig. 7. The value of k_h can be assumed as 1.5 times of k_v. For vacuum preloading, it is proposed that non-uniform consolidation of soils can be considered using the concept of equivalent smear effect with modified values of $k_h / k_h^{'}$ and s (Wang et al. 2020; Zhou and Chai 2017). To simiplify the problem, the equation $\mu_s = \ln\frac{n}{s}+\frac{k_h}{k_h^{'}}\ln s-\frac{3}{4}$ can be re-written as:

$$\mu_s = \ln n-\frac{3}{4}+\left(\frac{k_h}{k_h^{'}}-1\right)\ln s = \ln n-\frac{3}{4}+F_s \tag{3}$$

where F_s is the factor for accounting the overall smear effect. The smaller F_s, the higher speed of consolidation.

For vertical consolidation, the degree of consolidation $\bar{U}_v$ can be calculated by Terzaghi's one-dimensional consolidation theory (Terzaghi 1943), which will not be expanded here. With $\bar{U}_v$ and $\bar{U}_h$, the combined degree of consolidation U can be calculated by Eq.(4a) (Carrillo 1942) and the primary consolidation settlement $S_{"primary"}$ of HKMD under vacuum loading can be calculated by Eq.(4b).

$$U = 1-\left(1-\bar{U}_v\right)\left(1-\bar{U}_h\right) \tag{4a}$$

$$S_{"primary"} = U\frac{C_c}{1+e_0}H_0\log\frac{\sigma_z^{'}}{\sigma_{z0}^{'}} \tag{4b}$$

5.2 Calculation of settlement with a simplified Hypothesis B method

According to the widely accepted Hypothesis B, viscoplastic deformation (creep) occurs during the primary consolidation process (Leroueil et al. 1985; Kabbaj et al. 1988; Feng and Yin 2017; Feng et al. 2020; Chen et al. 2021). The creep deformation can be considered by adopting a simplified Hypothesis B method, firstly proposed by Yin and Feng (2017). The simplified method can be expressed as:

$$S_{totalB} = S_{"primary"} + \alpha \frac{C_\alpha}{1+e_0} H_0 \log \frac{t}{t_0} + \begin{cases} 0, \text{ for } t_0 \leq t < t_{EOP} \\ (1-\alpha) \frac{C_\alpha}{1+e_0} H_0 \log \frac{t}{t_{EOP}}, \text{ for } t_0 \leq t_{EOP} \leq t \end{cases} \quad (5)$$

where α is an empirical correction factor (frequently used as 0.8), C_α is the secondary consolidation coefficient, t_0 is the reference time (24 hours for the standad oedometer tests) and t_{EOP} is the time needed for end of primary consolidation in field ($U \approx 98\%$). When the loading time $t < t_{EOP}$, the final term will be zero. C_α is measured to be 0.0089 for 20 °C and 0.0078 for 40 °C under 50 kPa in the oedometer tests. All the parameters used in the calculations are listed in Table 1.

5.3 Effects of temperature on the consolidation settlement calculation

The effects of temperature on vacuum consolidation mainly include two parts. First of all, the undisturbed permeability is smaller under heating, as also indicated in oedometer tests. Secondly, as shown in the model tests, the effect of non-uniform consolidation is reduced under the higher temperature, which contributes to the value of F_s. Wang et al. (2020) suggested that $k_h / k_h^{'} = 6.3$ and $s = 4$ to consider the combined effect of clogging and non-uniform consolidation, for which F_s can be calculated as 7.35. For Model 2 with heating, F_s should be lower. The reduction of F_s may be attributed to significant improvement of permeability and concentrated heating at the filter-soil interface and soil column, which largely reduce the clogging and non-uniform consolidation under vacuum preloading, as discussed in the previous sections.

Fig. 21 shows the calculation results of consolidation settlements for the two models under vacuum pressure of 50 kPa with comparisons to measured data. The parameters determined from oedometer tests and different values of F_s are used for the calculation. It is found that $F_s = 7.35$ suggested by the literature can fit the result of Model 1 very well. For Model 2, $F_s = 1.5$ can best fit the settlement curves, despite of some unmatched points due to some simplifications and assumptions adopted in the calculation. Without modification of F_s, the calculated settlement curve of Model 2 develops faster than Model 1, but the settlement is still significantly underestimated. If F_s is taken as zero, the settlement is significantly overestimated. It seems that under the conditions in the present tests, the value of F_s is a dominant factor in the consolidation settlement of clayey soils.

6. Conclusions

In this study, oedometer and physical model tests were carried out on the thermal consolidation of HKMD at 20 °C and 40 °C respectively. The thermal effects on settlements, pore water pressure, vacuum loss, and water content are presented and discussed with molecular dynamic simulation and theoretical analysis. Several important remarks can be drawn as follows:

1) The consolidation of HKMD can be largely accelerated by heating. HKMD after vacuum-heat preloading exhibits larger consolidation settlement, lower water content, lower pore water pressure, and higher effective stress in a shorter period compared to vacuum preloading without heating.

2) Increasing the temperature can not only enhance the permeability of HKMD, but also reduce the effects of non-uniform consolidation and vacuum loss, which is the dominant factor to improve the efficiency of vacuum consolidation.

3) The results of molecular dynamic simulation demonstrate that the temperature plays an important effect in the transition of adsorbed water into free water, especially for MMT and MMT-Kao structures, which is less significant for Kao structure.

4) The settlements of HKMD under vacuum-heat preloading can be analyzed with Hansbo's solution and the simplified Hypothesis B method and the soil properties obtained from oedometer tests. The factor for smear effect F_s can be used to consider the combined effects of clogging, non-uniform consolidation, and heating, although further studies on investigating the general theoretical relations between temperature and consolidation under vacuum preloading are demanded.

Conflict of interest

No potential conflict of interest was reported by the authors.

Data Availability Statement

All data that support the findings of this study are available from the corresponding author upon reasonable request.

Acknowledgements

We are thankful for the financial support given by the Key Special Project for Introduced Talents Team of Southern Marine Science and Engineering Guangdong Laboratory (Guangzhou) (GML2019ZD0210), Project from Shenzhen Science and Technology Innovation Commission (JCYJ20210324105210028), the grand of Southern Marine Science and Engineering Guangdong Laboratory (Guangzhou) (K19313901). The work in this paper is also supported by General Research Fund (GRF) (PolyU 152179/18E, PolyU 152130/19E, project reference 15210020), a Research Impact Fund (R5037-18), and a Theme-based Resdearch Scheme project T22-502/18-R from Research Grants Council of Hong Kong Special Administrative Region Government of China. The work is also supported by grants (ZDBS and CD82) from The Hong Kong Polytechnic University, China.

References

Abuel-Naga, H. M., Bergado, D. T., & Chaiprakaikeow, S. (2006). Innovative thermal technique for enhancing the performance of prefabricated vertical drain during the preloading process. *Geotextiles and Geomembranes*, *24*(6), 359-370.

Abuel-Naga, H. M., Bergado, D. T., Bouazza, A., & Ramana, G. V. (2007). Volume change behaviour of saturated clays under drained heating conditions: experimental results and constitutive modeling. *Canadian Geotechnical Journal*, *44*(8), 942-956.

Abuel-Naga, H. M., Bergado, D. T., & Bouazza, A. (2008). Thermal conductivity evolution of saturated clay under consolidation process. *International Journal of Geomechanics*, *8*(2), 114-122.

Abuel-Naga, H. M., Bergado, D. T., Bouazza, A., & Pender, M. J. (2009). Thermal conductivity of soft Bangkok clay from laboratory and field measurements. *Engineering Geology*, *105*(3-4), 211-219.

Al-Zaoari, K., Zheng, Y. Y., Wei, P. C., Zhang, L. L., & Yin, Z. Y. (2022). Early stage of swelling process of dehydrated montmorillonite through molecular dynamics simulation. Materials Chemistry and Physics, 283, 126015.

Amarasinghe, P. M., & Anandarajah, A. (2012). Behavior of Swelling Clays: A Molecular Dynamic Study. *GeoCongress* 20122012. p. 2452-61.

Amarasinghe, P. M., & Anandarajah, A. (2013). Molecular Dynamic Study of the Swelling Behavior of Na-Montmorillonite. *Environmental and Engineering Geoscience*. *19*(2), 173-83.

Anderson, R. L., Ratcliffe, I., Greenwell, H. C., Williams, P. A., Cliffe, S, Coveney, P.V. (2010). Clay swelling — A challenge in the oilfield. *Earth-Science Reviews*. *98*(3-4) 201-16.

Artidteang, S., Bergado, D. T., Saowapakpiboon, J., Teerachaikulpanich, N., & Kumar, A. (2011). Enhancement of efficiency of prefabricated vertical drains using surcharge, vacuum and heat preloading. *Geosynthetics International*, *18*(1), 35-47.

Berendsen, H. J. C., Postma, J. P. M., van Gunsteren, W. F., & Hermans, J. (1981). Interaction Models for Water in Relation to Protein Hydration. In: *Pullman B, editor. Intermolecular Forces: Proceedings of the Fourteenth Jerusalem Symposium on Quantum Chemistry and Biochemistry Held in Jerusalem*, Israel, April 13–16, 1981. Dordrecht: Springer Netherlands, 1981. p. 331-42.

Bergado, D. T., Manivannan, R., & Balasubramaniam, A. S. (1996). Proposed criteria for discharge capacity of prefabricated vertical drains. *Geotextiles and Geomembranes*, *14*(9), 481-505.

Bergado, D. T., Sasanakul, I., & Horpibulsuk, S. (2003). Electro-osmotic consolidation of soft Bangkok clay using copper and carbon electrodes with PVD. *Geotechnical testing journal*, *26*(3), 277-288.

Baral, P., Indraratna, B., Rujikiatkamjorn, C., Kelly, R., & Vincent, P. (2021). Consolidation by Vertical Drains beneath a Circular Embankment under Surcharge and Vacuum Preloading. *Journal of Geotechnical and Geoenvironmental Engineering*, *147*(8), 05021004.

Cai, Y., Qiao, H., Wang, J., Geng, X., Wang, P., & Cai, Y. (2017). Experimental tests on effect of deformed prefabricated vertical drains in dredged soil on consolidation via vacuum preloading. *Engineering Geology*, *222*, 10-19.

Campanella, R. G., & Mitchell, J. K. (1968). Influence of temperature variations on soil behavior. *Journal of the Soil Mechanics and Foundations Division*, *94*(3), 709-734.

Cekerevac, C., Laloui, L., & Vulliet, L. (2002). Dependency law for thermal evolution of preconsolidation pressure. In *Proceedings of the 8th International Symposium on Numerical Models in Geomechanics, Rome, Italy, Edited by GN Pande and S. Pietruszczak. AA Balkema* (pp. 687-692).

Chai, J., Miura, N., & Bergado, D. T. (2008). Preloading clayey deposit by vacuum pressure with cap-drain: analyses versus performance. *Geotextiles and Geomembranes*, *26*(3), 220-230.

Chai, J., Carter, J. P., & Liu, M. D. (2014). Methods of vacuum consolidation and their deformation analyses. *Proceedings of the Institution of Civil Engineers-Ground Improvement*, *167*(1), 35-46.

Chang, F.-RC, Skipper, N. T., & Sposito, G. (1995). Computer Simulation of Interlayer Molecular Structure in Sodium Montmorillonite Hydrates. *Langmuir.* 11(7), 2734-41.

Chen, B., Huang, Y., Ye, W., Cui, Y., & Xu, Z. (2018, May). Investigation on the Thermal Conductivity of Shanghai Soft Clay. In *GeoShanghai International Conference* (pp. 984-992). Springer, Singapore.

Chen, Z. J., Feng, W. Q., & Yin, J. H. (2021). A new simplified method for calculating short-term and long-term consolidation settlements of multi-layered soils considering creep limit. *Computers and Geotechnics*, *138*, 104324.

Chien, S. C., Ou, C. Y., & Wang, M. K. (2009). Injection of saline solutions to improve the electro-osmotic pressure and consolidation of foundation soil. *Applied clay science*, *44*(3-4), 218-224.

Cho, W. J., Lee, J. O., & Chun, K. S. (1999). The temperature effects on hydraulic conductivity of compacted bentonite. *Applied clay science*, *14*(1-3), 47-58.

Cho, W. J., Lee, J. O., & Kwon, S. K. (2012). An analysis of the factors affecting the hydraulic conductivity and swelling pressure of Kyungju Ca-bentonite for use as a clay-based sealing material for a high-level waste repository. *Nuclear Engineering and Technology*, *44*(1), 89-102.

Chu, J., Yan, S. W., & Yang, H. (2000). Soil improvement by the vacuum preloading method for an oil storage station. *Geotechnique*, *50*(6), 625-632.

Cygan, R. T., Greathouse, J. A., Heinz, H., & Kalinichev, A. G. (2009). Molecular models and simulations of layered materials. *Journal of Materials Chemistry. 19*(17), 2470-81.

Cygan, R. T., Liang, J.-J., & Kalinichev, A. G. (2004). Molecular Models of Hydroxide, Oxyhydroxide, and Clay Phases and the Development of a General Force Field. *The Journal of Physical Chemistry B. 108*(4), 1255-66.

Delage, P., Sultan, N., & Cui, Y. J. (2000). On the thermal consolidation of Boom clay. *Canadian Geotechnical Journal*, *37*(2), 343-354.

Delage, P., Sultan, N., Cui, Y. J., & Ling, L. X. (2011). Permeability changes in Boom clay with temperature. *arXiv preprint arXiv:1112.6396*.

Deng, A., & Xu, S. L. (2010). Consolidating dredge soil by combining vacuum and dynamic compaction effort. In *Ground Improvement and Geosynthetics* (pp. 113-118).

Du, C., Hu, X., Fu, H., & Wang, J. (2021). Effects of temperature circulation on dredged sludge improved by vacuum preloading. *Soils and Foundations, 61*(5), 1343-1353.

Du, D. J., Yang, A. W., & Liu, J. (2010). Blow-filled Reclamations in Tianjin Coastal Regions. Science Press, Beijing (in Chinese)

Feng, S. J., Du, F. L., Chen, H. X., & Mao, J. Z. (2017). Centrifuge modeling of preloading consolidation and dynamic compaction in treating dredged soil. *Engineering Geology*, *226*, 161-171.

Feng, W. Q., Yin, J. H., Chen, W. B., Tan, D. Y., & Wu, P. C. (2020). A new simplified method for calculating consolidation settlement of multi-layer soft soils with creep under multi-stage ramp loading. *Engineering Geology*, *264*, 105322.

Hansbo, S. (1981). Consolidation of fine-grained soils by prefabricated drains. *Proc. 10th ICSMFE, 1981*, *3*, 677-682.

Indraratna, B., Bamunawita, C., & Khabbaz, H. (2004). Numerical modeling of vacuum preloading and field applications. *Canadian Geotechnical Journal*, *41*(6), 1098-1110.

Indraratna, B., Rujikiatkamjorn, C., & Sathananthan, I. (2005). Analytical and numerical solutions for a single vertical drain including the effects of vacuum preloading. *Canadian Geotechnical Journal*, *42*(4), 994-1014.

Jarad, N. (2016). *Temperature impact on the consolidation and creep behaviour of compacted clayey soils* (Doctoral dissertation, Université de Lorraine).

Jeyakanthan, V., Gnanendran, C. T., & Lo, S. C. (2011). Laboratory assessment of electro-osmotic stabilization of soft clay. *Canadian Geotechnical Journal*, *48*(12), 1788-1802.

Kabbaj, M., Tavenas, F., & Leroueil, S. (1988). In situ and laboratory stress–strain relationships. *Géotechnique*, *38*(1), 83-100.

Laloui, L., Leroueil, S., & Chalindar, S. (2008). Modelling the combined effect of strain rate and temperature on one-dimensional compression of soils. *Canadian Geotechnical Journal*, *45*(12), 1765-1777.

Leroueil, S., Kabbaj, M., Tavenas, F., & Bouchard, R. (1985). Stress–strain–strain rate relation for the compressibility of sensitive natural clays. *Géotechnique*, *35*(2), 159-180.

Liu, L., He, H., Dyck, M., & Lv, J. (2021). Modeling thermal conductivity of clays: A review and evaluation of 28 predictive models. *Engineering Geology,* 106107.

Lin, Z. Q. (2015). Changing rules of pore water pressure in drain board under vacuum preloading. *Port & Waterway Engineering*, *7*, 161-166.

Long, R. P., & Covo, A. (1994). Equivalent diameter of vertical drains with an oblong cross section. *Journal of Geotechnical Engineering*, *120*(9), 1625-1630.

Ma, X., Fan, Y., Dong X., Chen, R., Li, H., & Sun, D., et al. (2018). Impact of Clay Minerals on the Dewatering of Coal Slurry: An Experimental and Molecular-Simulation Study. *Minerals. 8*(9). 400; https://doi.org/10.3390/min8090400

Menard, L., & Broise, Y. (1975). Theoretical and practical aspect of dynamic consolidation. *Geotechnique*, *25*(1), 3-18.

Park, H. I., Kim, K. S., & Kim, H. Y. (2015). Field performance of a genetic algorithm in the settlement prediction of a thick soft clay deposit in the southern part of the Korean peninsula. *Engineering Geology*, *196*, 150-157.

Perera, D., Indraratna, B., Leroueil, S., Rujikiatkamjorn, C., & Kelly, R. (2017). Analytical model for vacuum consolidation incorporating soil disturbance caused by mandrel-driven drains. *Canadian Geotechnical Journal*, *54*(4), 547-560.

Plimpton, S. (1995). Fast Parallel Algorithms for Short-Range Molecular Dynamics. *Journal of Computational Physics*. *117*(1), 1-19.

Saowapakpiboon, J., Bergado, D. T., & Artidteang, S. (2011). Comparison on the performance of prefabricated vertical drain (PVD) preloading combined with and without vacuum and heat. *Lowland Technology International*, *13*(1, June), 2-9.

Stukowski, A. (2009). Visualization and analysis of atomistic simulation data with OVITO–the Open Visualization Tool. *Modelling and Simulation in Materials Science and Engineering. 18*(1), 015012.

Sun, H. L., Weng, Z. Q., Liu, S. J., Geng, X. Y., Pan, X. D., Cai, Y. Q., & Shi, L. (2020). Compression and consolidation behaviors of lime-treated dredging slurry under vacuum pressure. *Engineering Geology*, *270*, 105573.

Tavenas, F., Jean, P., Leblond, P., & Leroueil, S. (1983). The permeability of natural soft clays. Part II: Permeability characteristics. *Canadian Geotechnical Journal*, *20*(4), 645-660.

Tsutsumi, A., & Tanaka, H. (2012). Combined effects of strain rate and temperature on consolidation behavior of clayey soils. *Soils and Foundations, 52*(2), 207-215.

Wan, T. Y., & Mitchell, J. K. (1976). Electro-osmotic consolidation of soils. *Journal of the Geotechnical Engineering Division*, *102*(5), 473-491.

Wang, J., Cai, Y., Ma, J., Chu, J., Fu, H., Wang, P., & Jin, Y. (2016). Improved vacuum preloading method for consolidation of dredged clay-slurry fill. *Journal of Geotechnical and Geoenvironmental Engineering*, *142*(11), 06016012.

Wang, J., Ni, J., Cai, Y., Fu, H., & Wang, P. (2017). Combination of vacuum preloading and lime treatment for improvement of dredged fill. *Engineering Geology*, *227*, 149-158.

Wang, J., Cai, Y., Fu, H., Hu, X., Cai, Y., Lin, H., & Zheng, W. (2018). Experimental study on a dredged fill ground improved by a two-stage vacuum preloading method. *Soils and Foundations*, *58*(3), 766-775.

Wang, J., Zhao, R., Cai, Y., Fu, H., Li, X., & Hu, X. (2018). Vacuum preloading and electro-osmosis consolidation of dredged slurry pre-treated with flocculants. *Engineering Geology*, *246*, 123-130.

Wang, J., Huang, G., Fu, H., Cai, Y., Hu, X., Lou, X., Jin, Y., Hai, J., Ni, J., & Zou, J. (2019). Vacuum preloading combined with multiple-flocculant treatment for dredged fill improvement. *Engineering Geology*, *259*, 105194.

Wang, P., Han, Y., Zhou, Y., Wang, J., Cai, Y., Xu, F., & Pu, H. (2020). Apparent clogging effect in vacuum-induced consolidation of dredged soil with prefabricated vertical drains. *Geotextiles and Geomembranes*, *48*(4), 524-531.

Wang, H., Wu, S., Qi, X., & Chu, J. (2021). Site characterization of reclaimed lands based on seismic cone penetration test. *Engineering Geology*, *280*, 105953.

Wu, Z., Deng, Y., Cui, Y., Chu, C., & Feng, Q. (2020). Geological investigation of the settlement behaviour of two highways in Lianyungang region. *Engineering Geology*, *272*, 105648.

Xu, B. H., He, N., Jiang, Y. B., Zhou, Y. Z., & Zhan, X. J. (2020). Experimental study on the clogging effect of dredged fill surrounding the PVD under vacuum preloading. *Geotextiles and Geomembranes*, *48*(5), 614-624.

Yim, W. S. (1994). Offshore Quaternary sediments and their engineering significance in Hong Kong. *Engineering Geology*, *37*(1), 31-50.

Yin, J. H., & Feng, W. Q. (2017). A new simplified method and its verification for calculation of consolidation settlement of a clayey soil with creep. *Canadian Geotechnical Journal*, *54*(3), 333-347.

Zhan, T. L., Zhan, X., Lin, W., Luo, X., & Chen, Y. (2014). Field and laboratory investigation on geotechnical properties of sewage sludge disposed in a pit at Changan landfill, Chengdu, China. *Engineering geology*, *170*, 24-32.

Zhou, Y., Cai, Y., Yuan, G., Wang, J., Fu, H., Hu, X., ... & Jin, H. (2021). Effect of tamping interval on consolidation of dredged slurry using vacuum preloading combined with dynamic consolidation. *Acta Geotechnica*, *16*(3), 859-871.

Zhou, Y., & Chai, J. C. (2017). Equivalent ‘smear’effect due to non-uniform consolidation surrounding a PVD. *Géotechnique*, *67*(5), 410-419.

Caption of Figures

Fig. 1 The systematic structures and internal connection of this study

Fig. 2 Schematical drawing of the thermal oedometer test

Fig. 3 Test set-up of the vacuum-heat preloading system

Fig. 4 Particle size distribution curve of HKMD

Fig. 5 $e - \log \sigma_z^{'}$ curves of HKMD in different temperatures from oedometer tests

Fig. 6 $e - \log t$ curves of HKMD under different loadings and temperatures in oedometer

Fig. 7 $e - \log k_v$ curves of HKMD in different temperatures from oedometer tests

Fig. 8 Measured temperature at three different positions in Model 2

Fig. 9 Settlement curves after self-consolidation calculated by discharged water

Fig. 10 Settlement curves measured by LVDTs

Fig. 11 Measured pore water pressure with time at different positions in two model tests

Fig. 12 Measured vacuum pressure at the middle of PVD

Fig. 13 Photos of the bent PVDs after tests

Fig. 14 Microscopic photos of the PVDs after tests: (a) Model 1, 9.5x magnification; (b) Model 2, 9.5x magnification; (b) Model 1, 60x magnification; and (d) Model 2, 60x magnification

Fig. 15 Schematic diagram of the clogging effect on vacuum pressure measuring on a cross-section of PVD

Fig. 16 Water content of two tests before and after vacuum loading

Fig. 17 Microstructure of HKMD from SEM and three typical molecular simulation models: (a) MMT, (b) Kao, and (c) MMT-Kao model

Fig. 18 Trajectory line of water molecular during the simulation in Kao model at 20 °C

Fig. 19 Density distribution of water along the z direction of MMT-Kao model

Fig. 20 The transit percent of adsorbing water on the clay surface at 20, 40 and 80 °C: (a) MMT, (b) Kao, and (c) MMT-Kao model

Fig. 21 Relations of total vertical settlement and log(time) of the two physical model tests from measurement and calculations

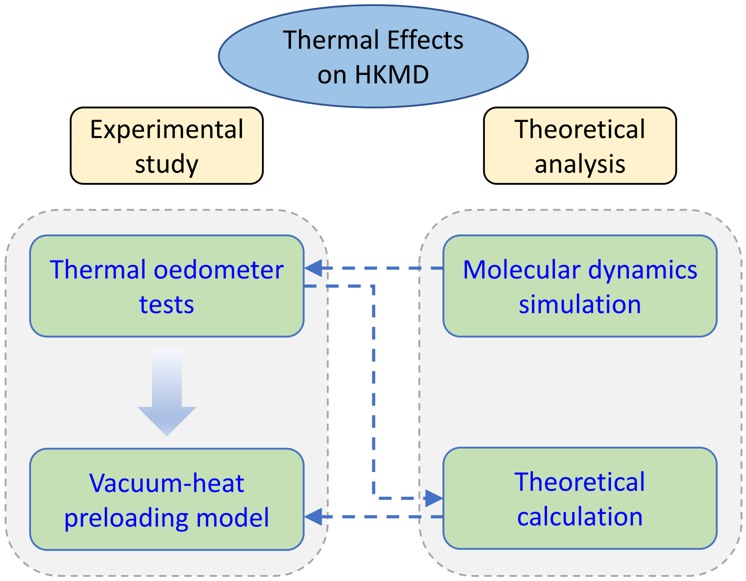

Fig. 1 The systematic structures and internal connection of this study

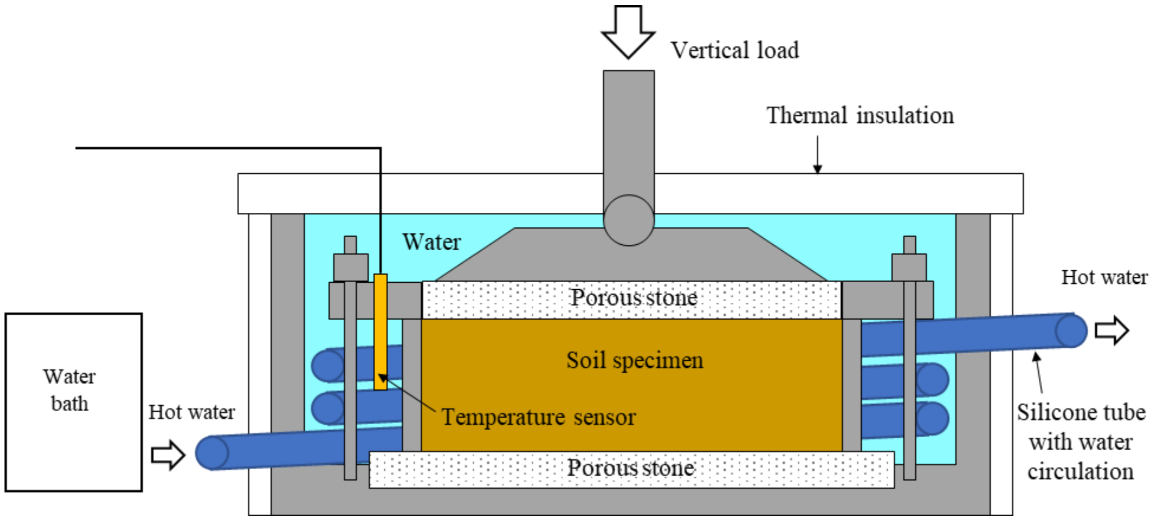

Fig. 2 Schematical drawing of the thermal oedometer test

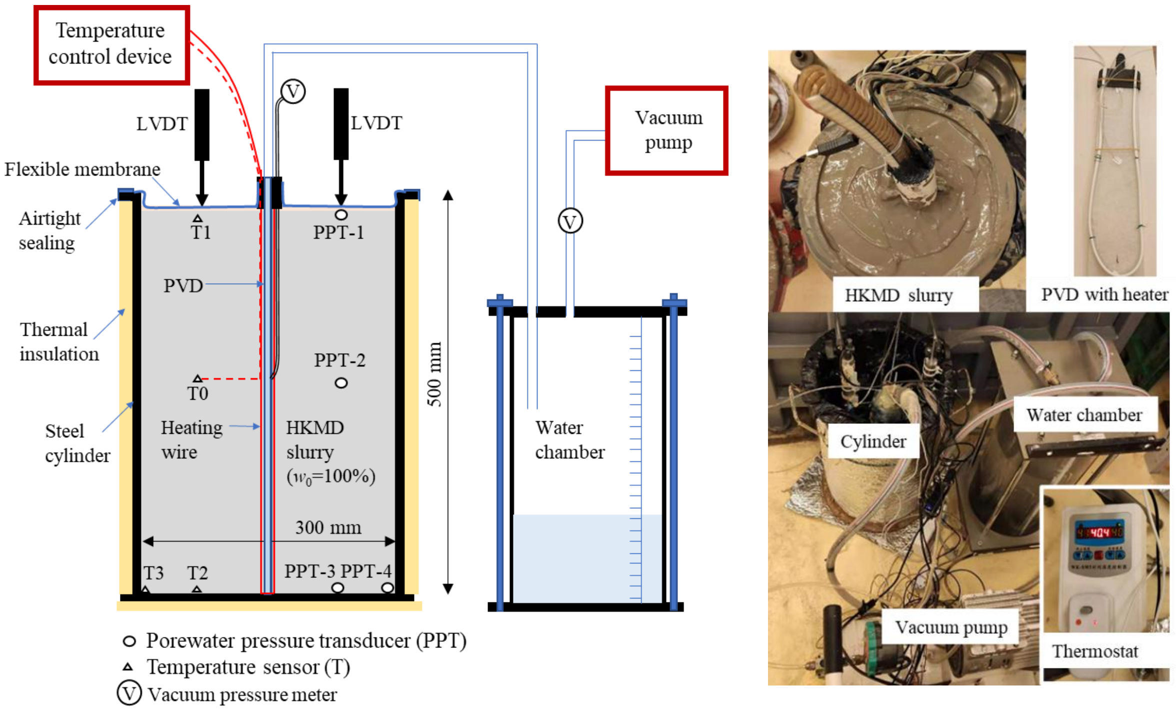

Fig. 3 Test set-up of the vacuum-heat preloading system

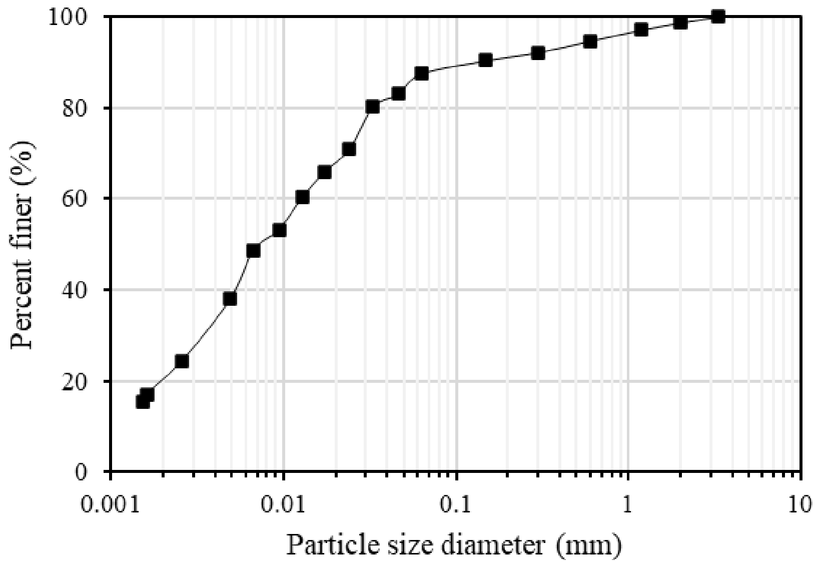

Fig. 4 Particle size distribution curve of HKMD

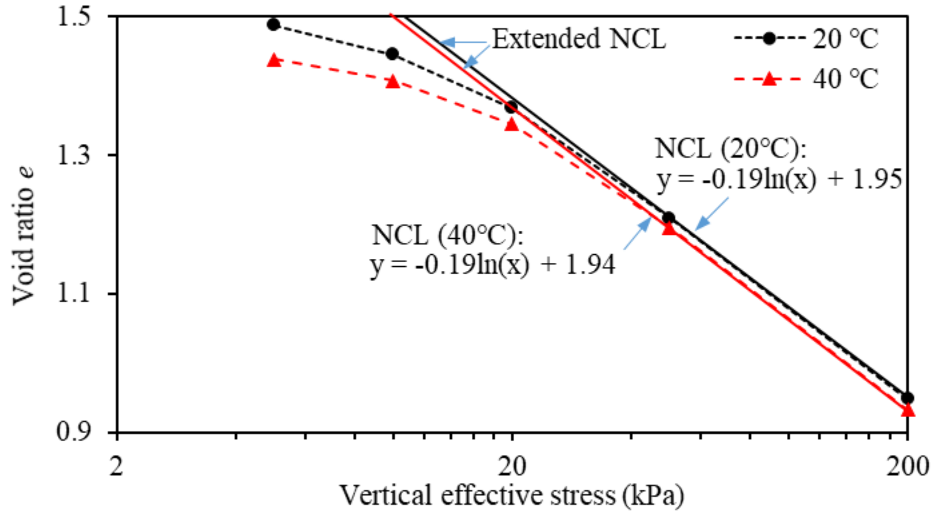

Fig. 5 $e - \log \sigma_z^{'}$ curves of HKMD in different temperatures from oedometer tests

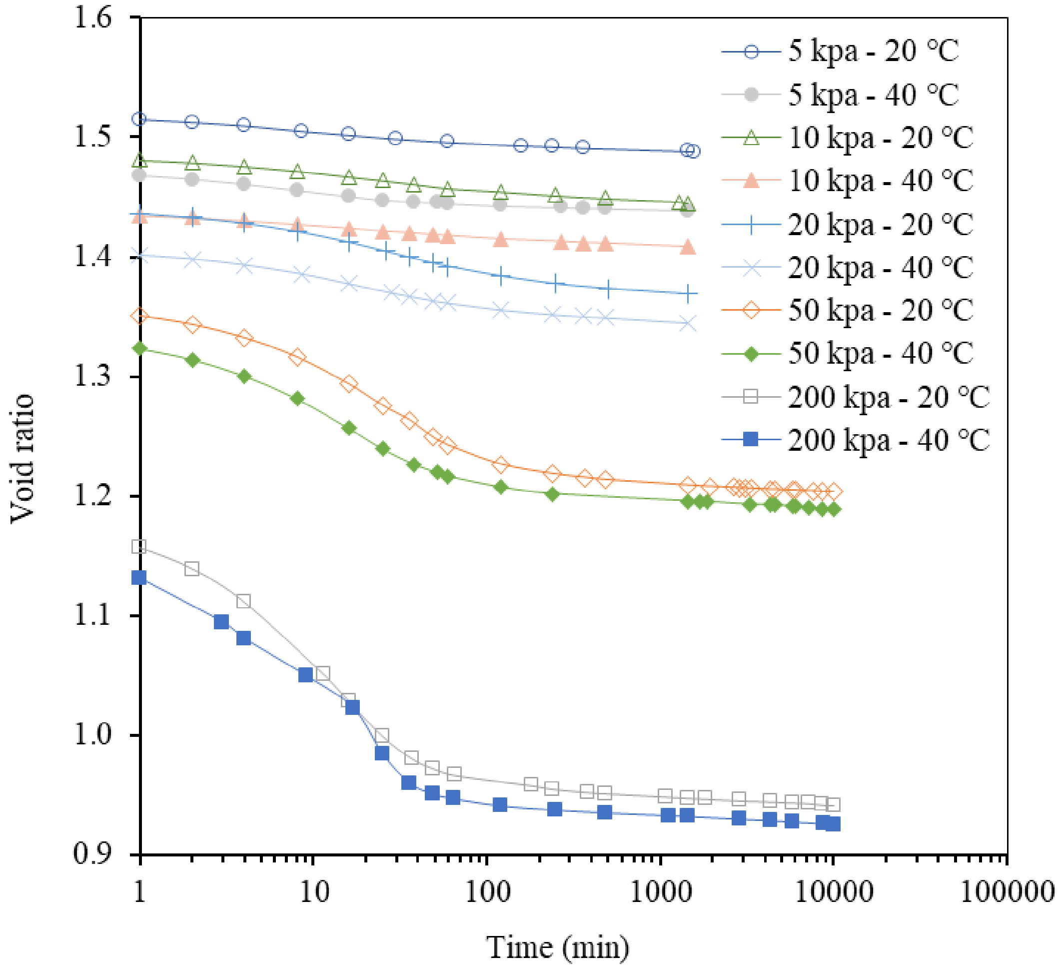

Fig. 6 $e-\log t$ curves of HKMD under different loadings and temperatures in oedometer

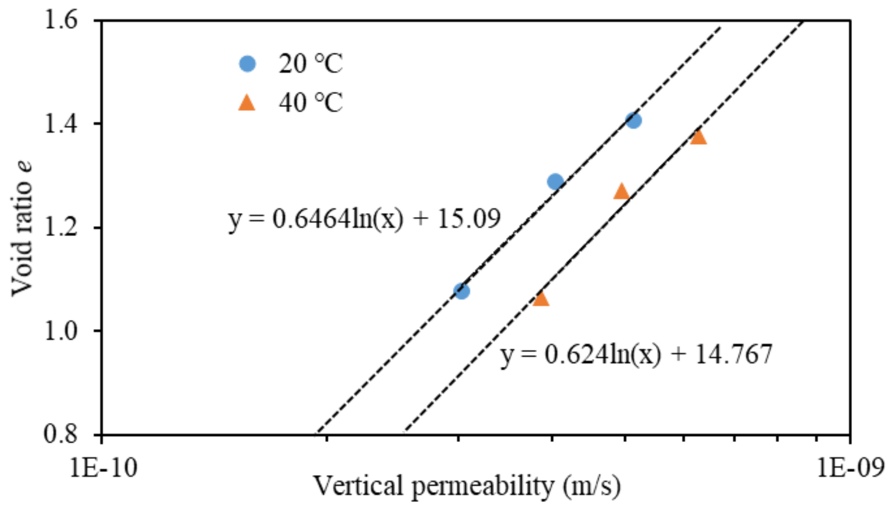

Fig. 7 $e-\log k_v$ curves of HKMD in different temperatures from oedometer tests

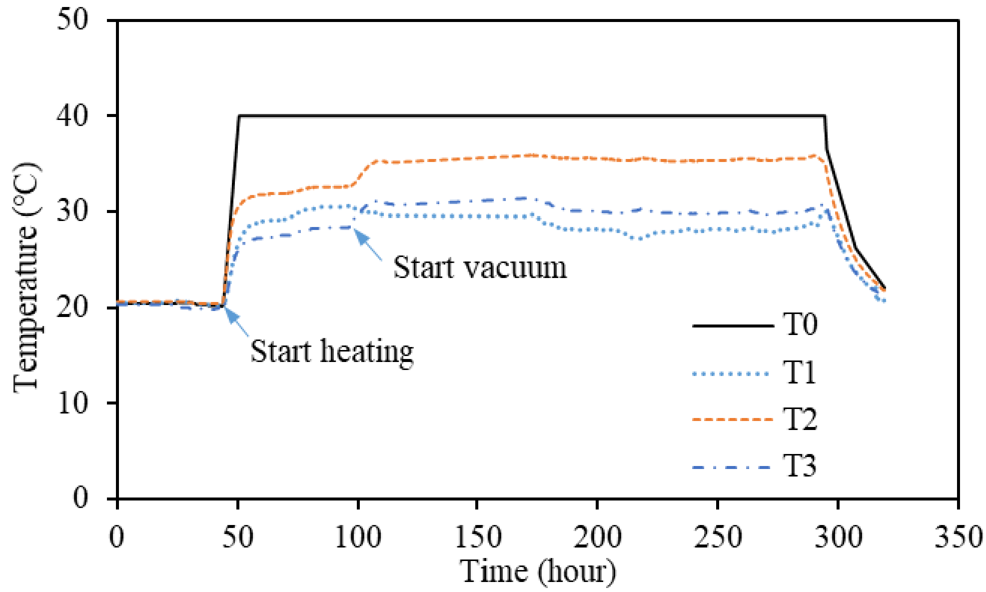

Fig. 8 Measured temperature at three different positions in Model 2

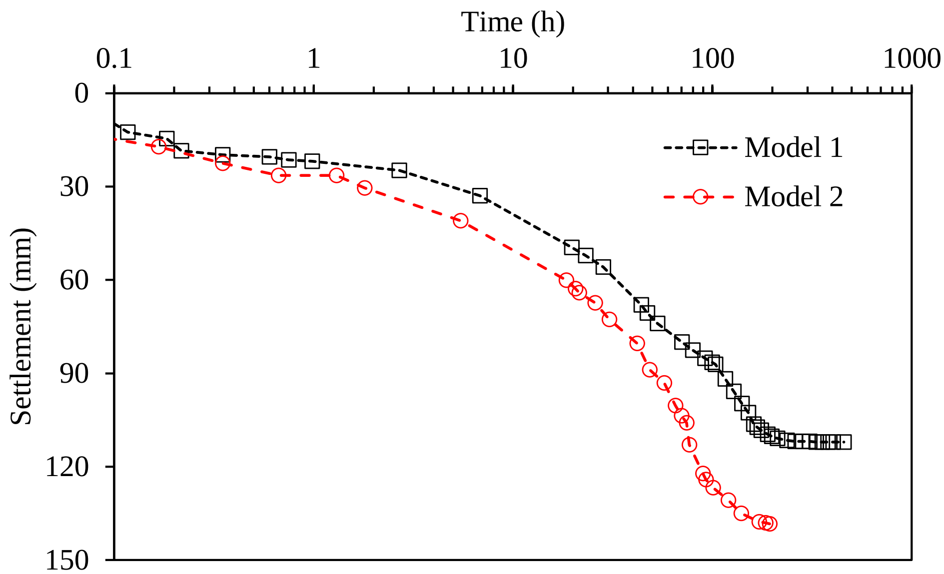

Fig. 9 Settlement curves after self-consolidation calculated by discharged water

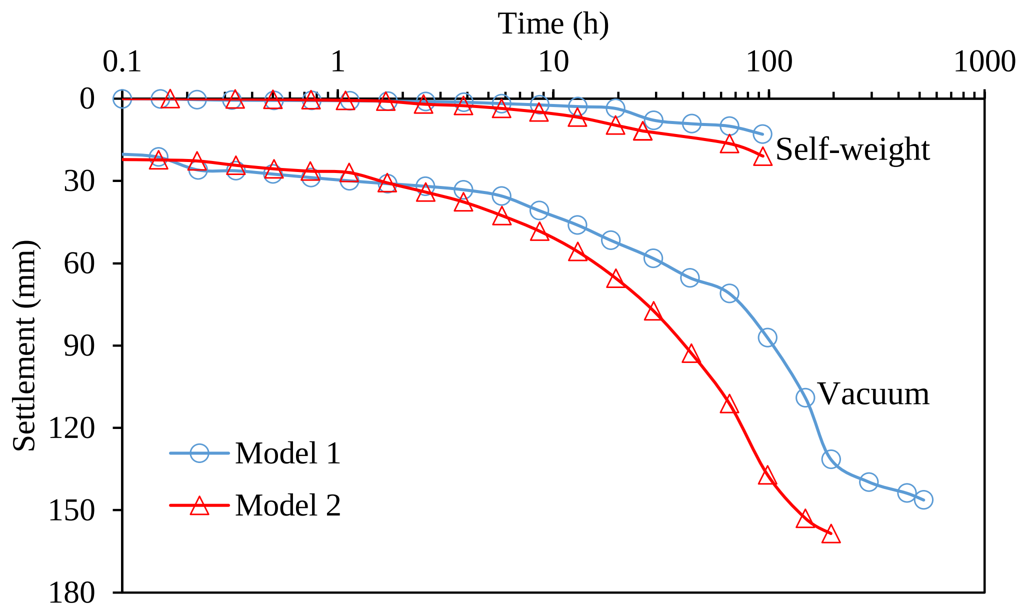

Fig. 10   Settlement curves measured by LVDTs

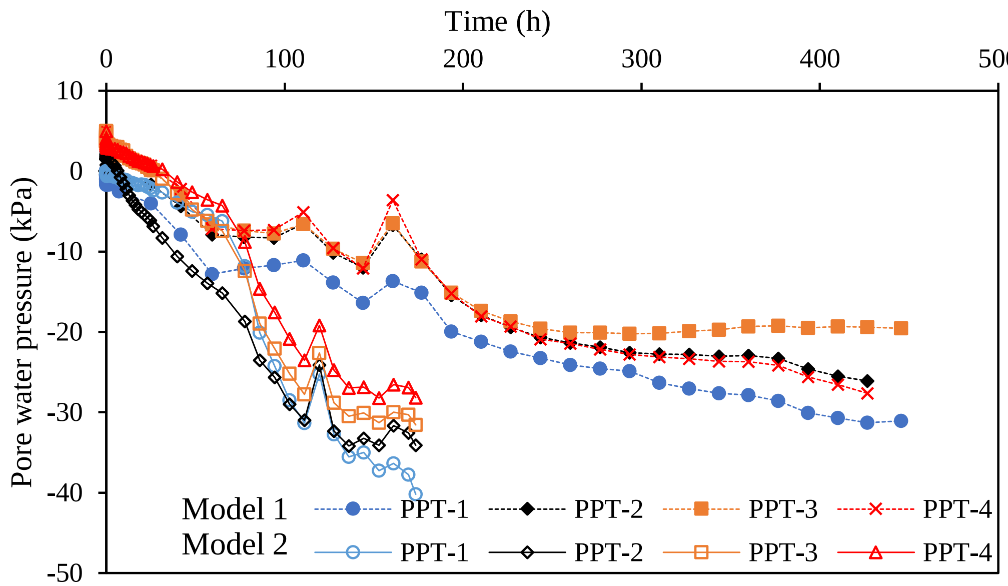

Fig. 11 Measured pore water pressure with time at different positions in two model tests

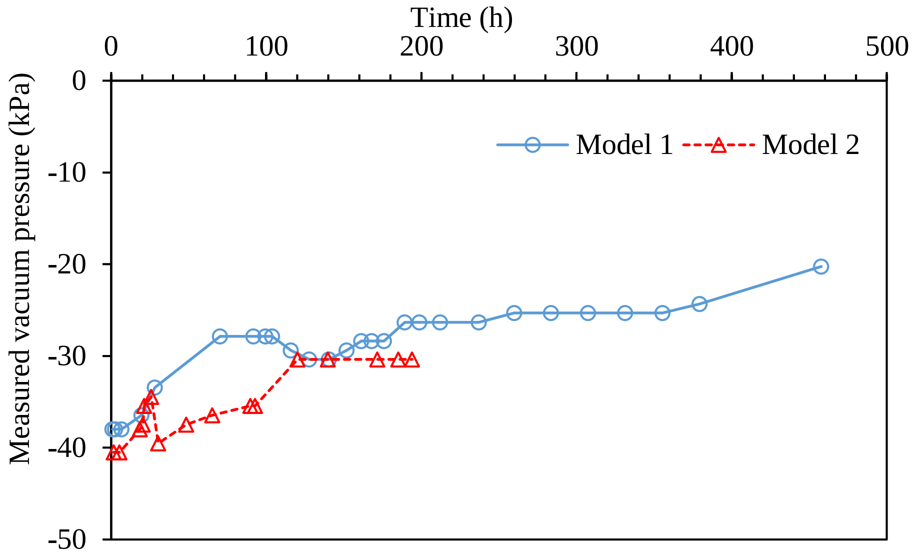

Fig. 12 Measured vacuum pressure at the middle of PVD

Fig. 13   Photos of the bent PVDs after tests

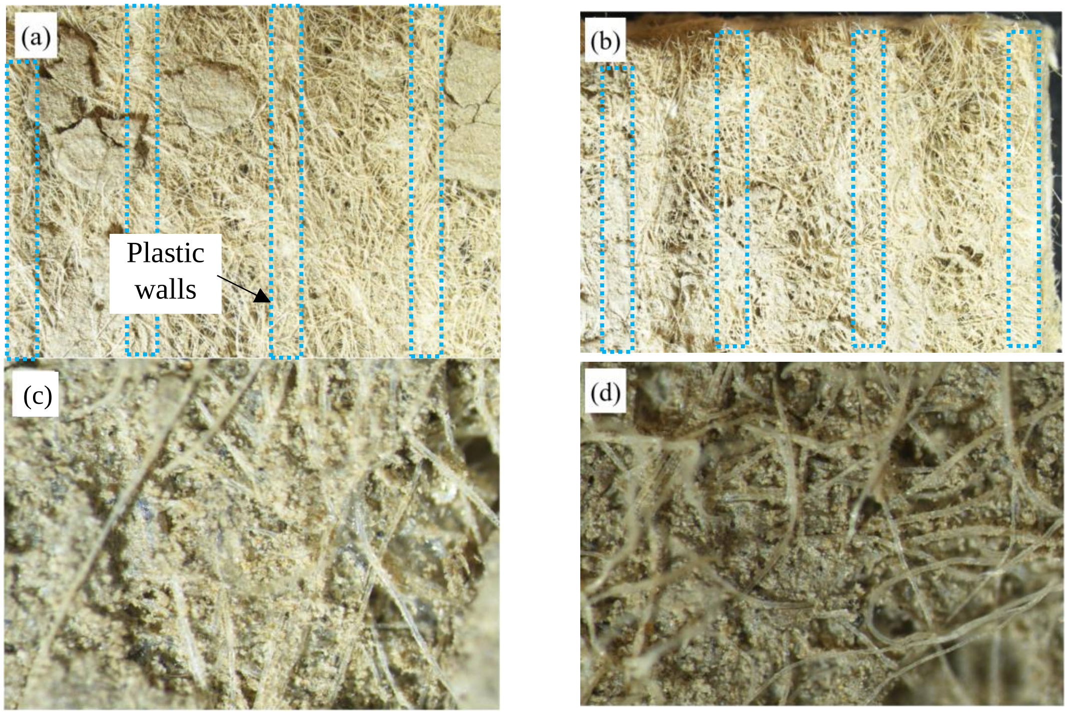

Fig. 14 Microscopic photos of the PVDs after tests: (a) Model 1, 9.5x magnification; (b) Model 2, 9.5x magnification; (b) Model 1, 60x magnification; and (d) Model 2, 60x magnification

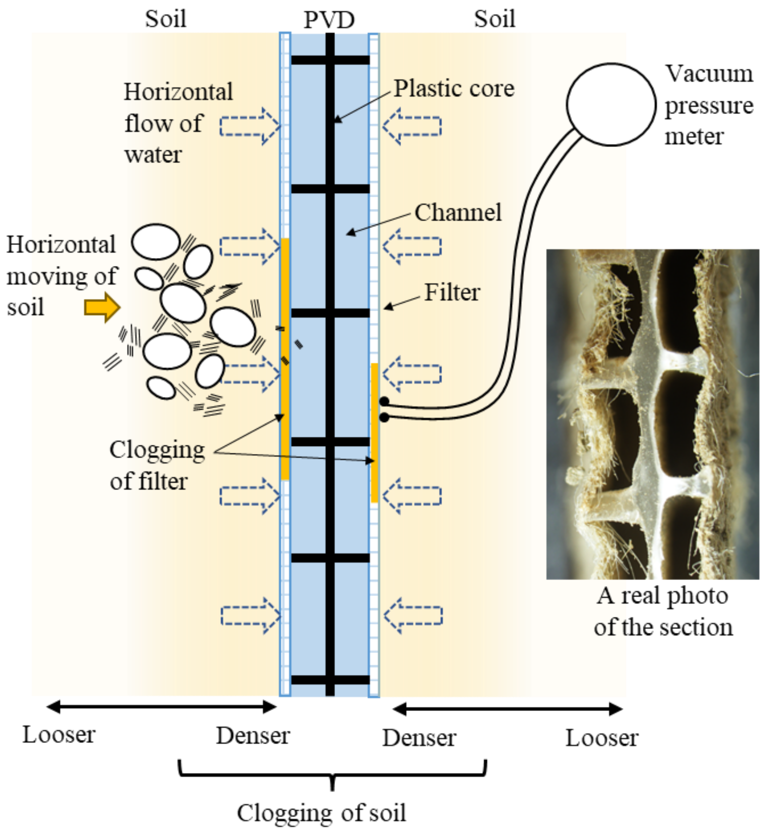

Fig. 15 Schematic diagram of the clogging effect on vacuum pressure measuring on a cross-section of PVD

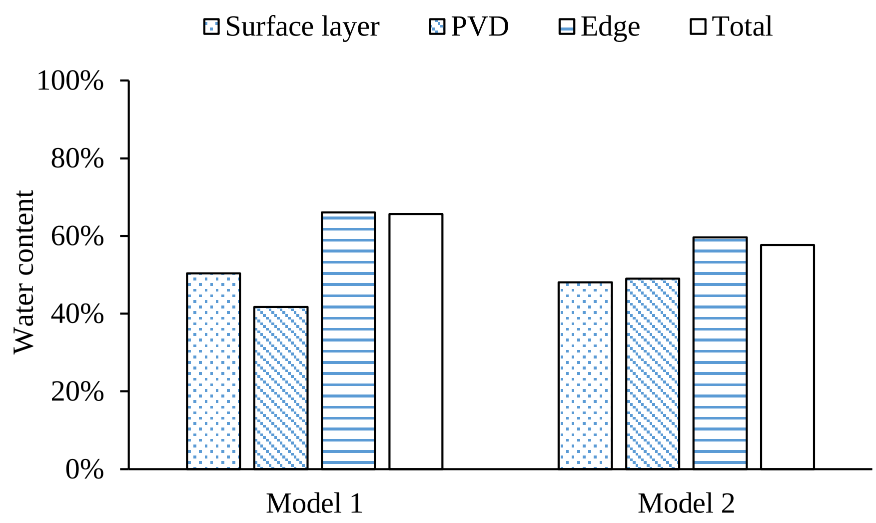

Fig. 16   Water content of two tests before and after vacuum loading

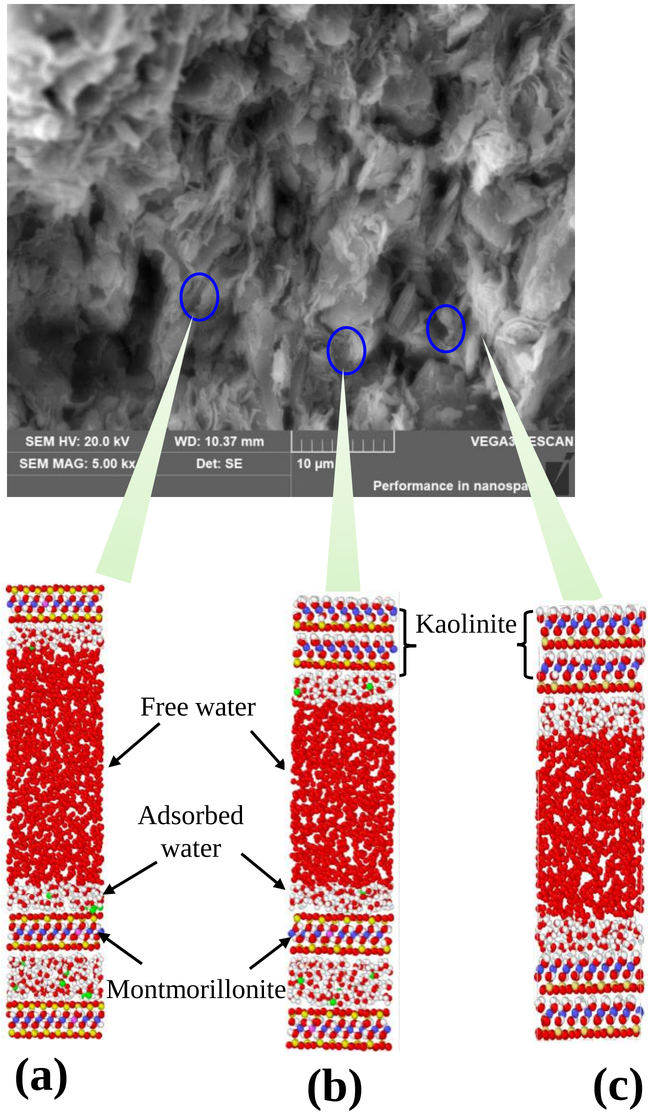

Fig. 17 Microstructure of HKMD from SEM and three typical molecular simulation models: (a) MMT, (b) Kao and (c) MMT-Kao model

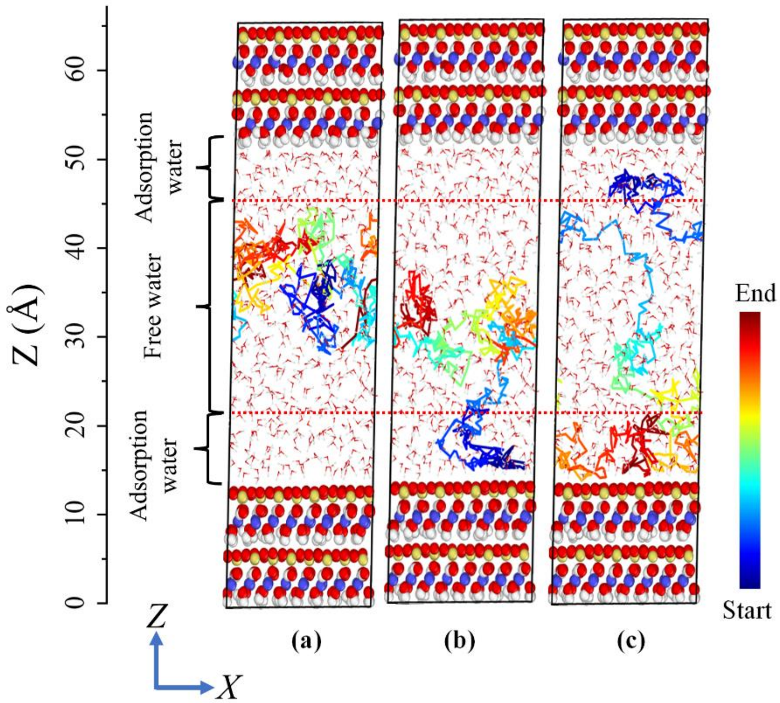

Fig. 18 Trajectory line of water molecular during the simulation in Kao model

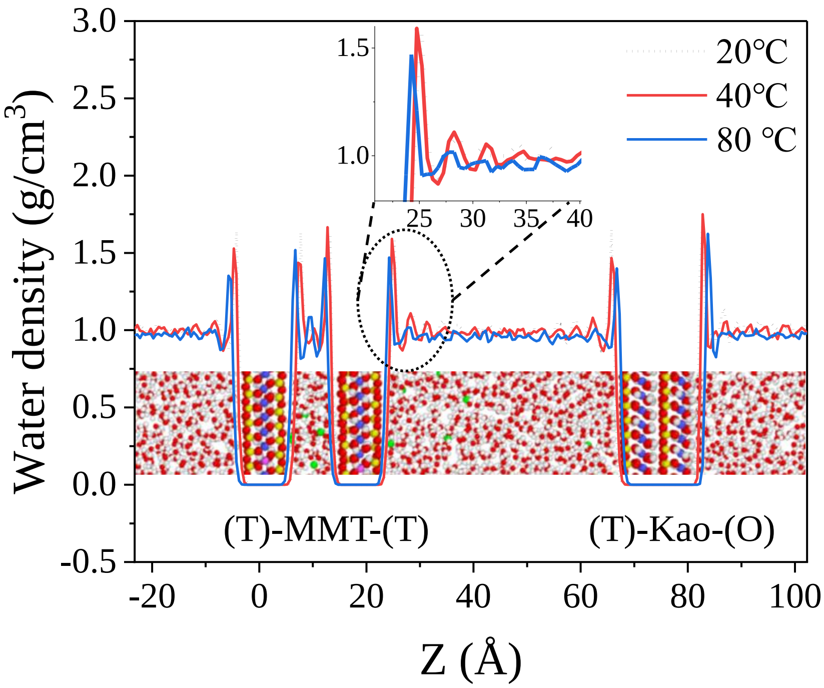

Fig. 19   Density distribution of water along the z direction of MMT-Kao model

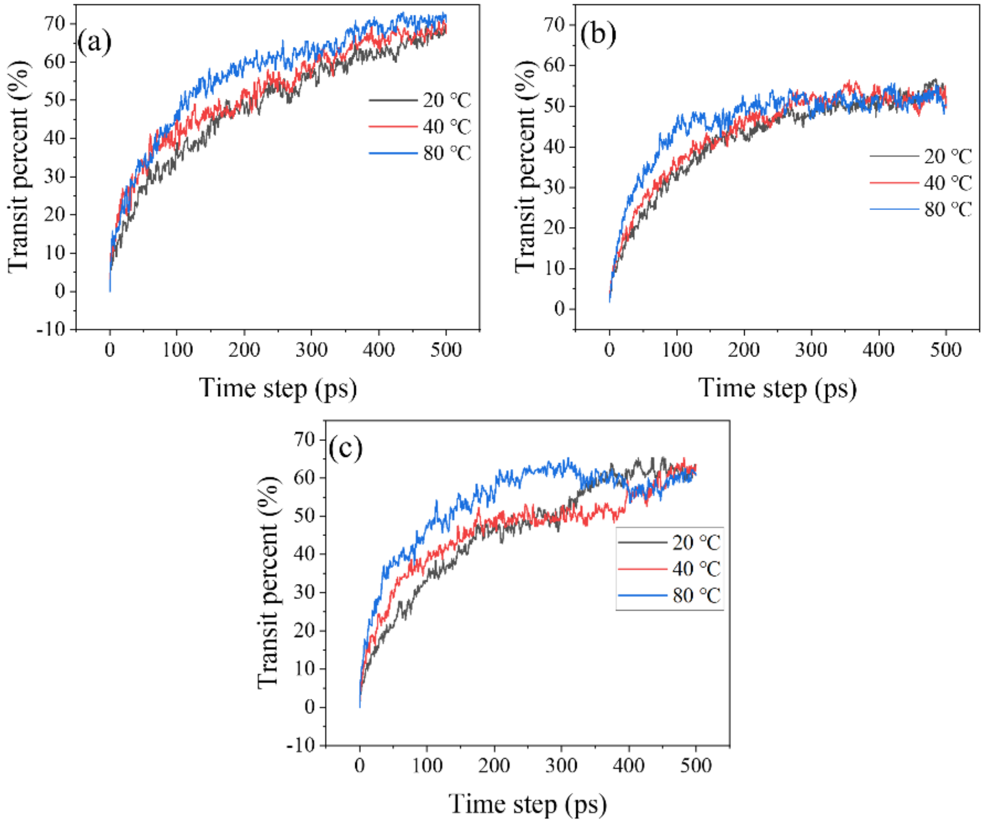

Fig. 20 The transit percent of adsorbing water on the clay surface at 20, 40 and 80 °C: (a) MMT, (b) Kao, and (c) MMT-Kao model

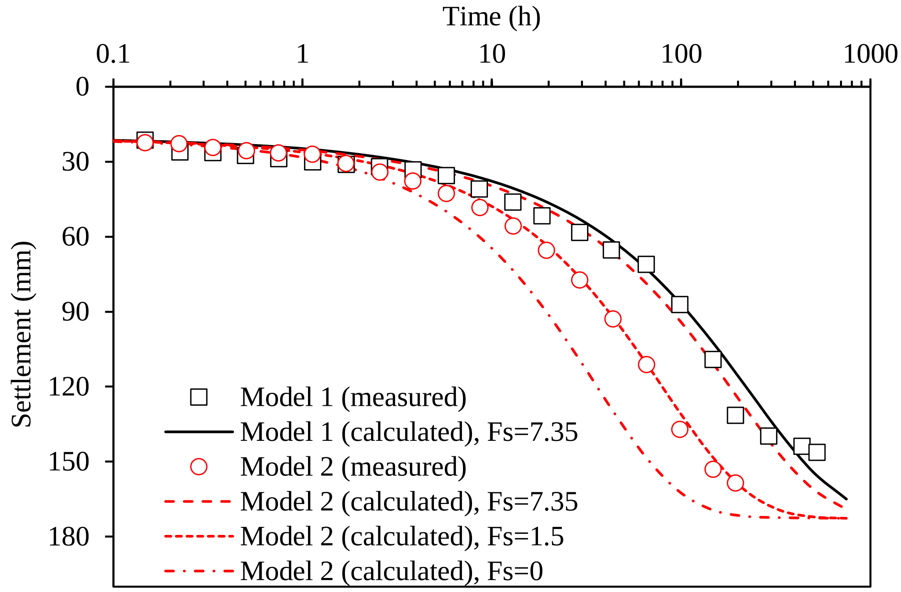

Fig. 21 Relations of total vertical settlement and log(time) of the two physical model tests from measurement and calculations

Table 1 Parameters for consolidation settlement calculation

T (°C)	H (m)	D (m)	d_w (m)	d_s (m)	N	C_c	C_α	e_0	k_v (m/s)	k_h (m/s)	F_s
20	0.45	0.294	0.0535	0.214	1.95	0.433	0.0089	2.49	2.83×10^{-9}	4.24×10^{-9}	7.35
40	0.45	0.294	0.0535	0.214	1.94	0.437	0.0078	2.49	3.37×10^{-9}	5.06×10^{-9}	1.50